LA-UR- 07-7240

Approved for public release;
distribution is unlimited.

Title: Collimators for the BDD-IIRM, the Modified Burst Detection Dosimeter for Block IIR Satellites of the Global Positioning System

Author(s): Thomas E. Cayton
John E. Valencia

Intended for: Workshop on Radiation Belt Data
Lacanau, France
12-16 November 2007

Form 836 (7/06)

Collimators for the BDD-IIRM, the Modified Burst Detection Dosimeter for Block IIR Satellites of the Global Positioning System

by

Thomas E. Cayton and John E. Valencia

Abstract

The on-orbit performance of the first BDD-IIR (Burst Detection Dosimeter, Block IIR) instrument that flew aboard GPS NS41 (Global Positioning System satellite Navstar 41), demonstrated a design flaw in the "saltshaker" shields employed in four of the instrument's eight channels: sun light heavily contaminated the data reported by one of these channels. In response to the identified vulnerability to light leaks, the two remaining BDD-IIR instruments were modified by replacing all of the collimators of the saltshaker type by new ones of a more robust design, with identical masses and fabricated mostly from spare parts. In addition to eliminating light leaks, the new collimators were designed to improve the contrast between the direct-electron component and the secondary-bremsstrahlung component of the detector response. The original saltshaker shields of the BDD-IIR on NS41 are compared and contrasted with the replacement collimators deployed in the BDD-IIRM for the second flight unit and the flight spare.

1. Instrument Description

The BDD-IIR[1] features eight individual channels of a "shield/filter/sensor" design that permits the instrument to sample roughly half of the celestial sphere (and thus to monitor the omnidirectional flux) while at the same time protecting the silicon sensor elements from most of the incident particle flux. Three types of shield/filters were deployed on the BDD-IIR, two thick hemispherical domes, four "saltshaker" shields, and two conical collimators. The energy range covered by each of the eight channels is determined by the design of the shield and the filter; the silicon sensor elements themselves and their signal-processing electronics are identical to within the tolerances of the individual components.

The four BDD-IIR saltshaker shields are depicted in Figs. 1 to 4, where the various colors indicate the materials from which instrument is constructed, as follows. The silicon sensor element is shown in purple; beryllium shield and filters, yellow; gold shield and collimators, red; titanium support ring, blue; plastic insulation, green; and lumped mass below the sensor deck; magenta. The aluminum instrument housing and sensor deck (approximated here as a simple hemispherical shell and annulus) are shown in gray. For each of the saltshaker shields, particles are admitted to the sensor through five radially-oriented, cylindrical gold collimators that pierce a thick beryllium and gold dome shield, one at 0° and four equally-spaced at 45°. Beryllium filters at the bottoms of the collimating apertures determine the energy range covered by each channel; achieving and maintaining a light-tight interface at this point proved to be too much of a challenge for the simple glue-together construction method attempted with the BDD-IIR.

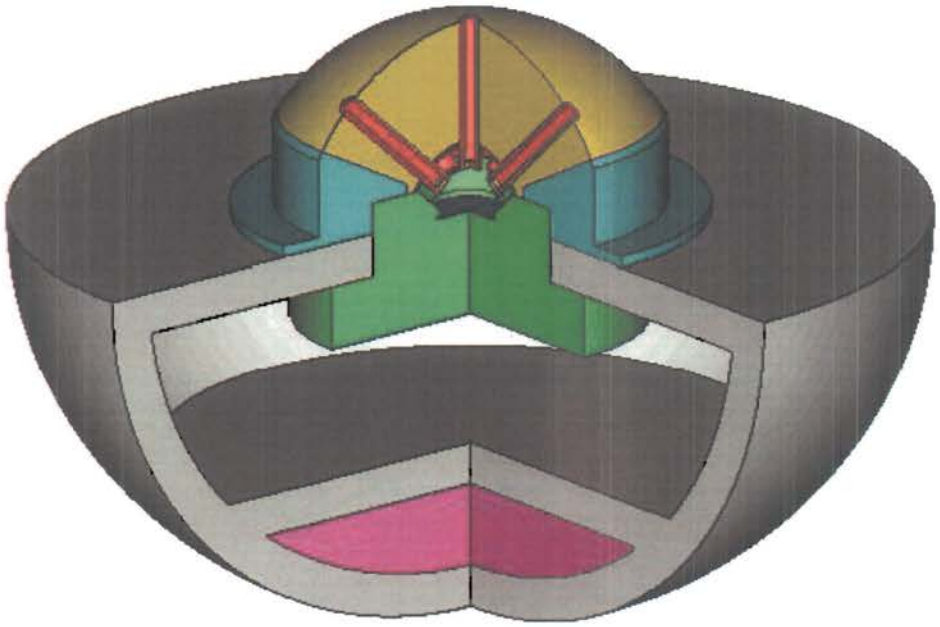

Figure 1. Saltshaker shield for channel 3 as flown on the BDD-IIR on NS41

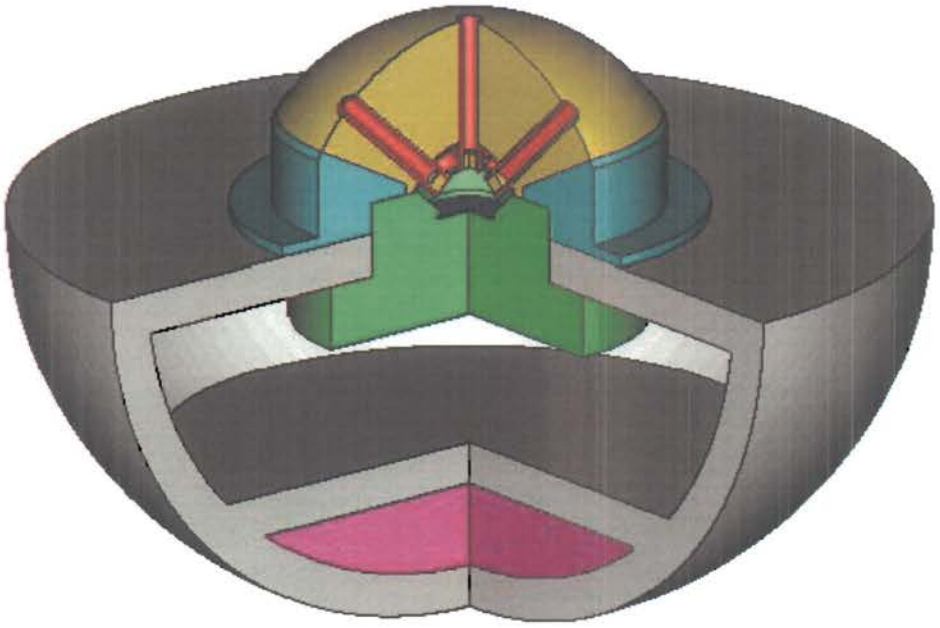

Figure 2. Saltshaker shield for channel 4 as flown on the BDD-IIR on NS41

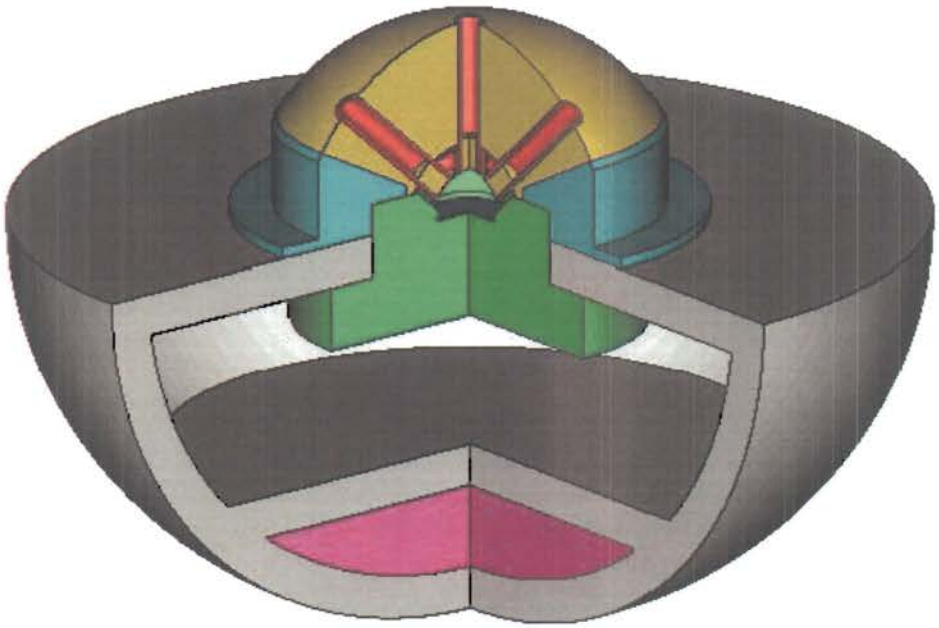

Figure 3. Saltshaker shield for channel 5 as flown on the BDD-IIR on NS41

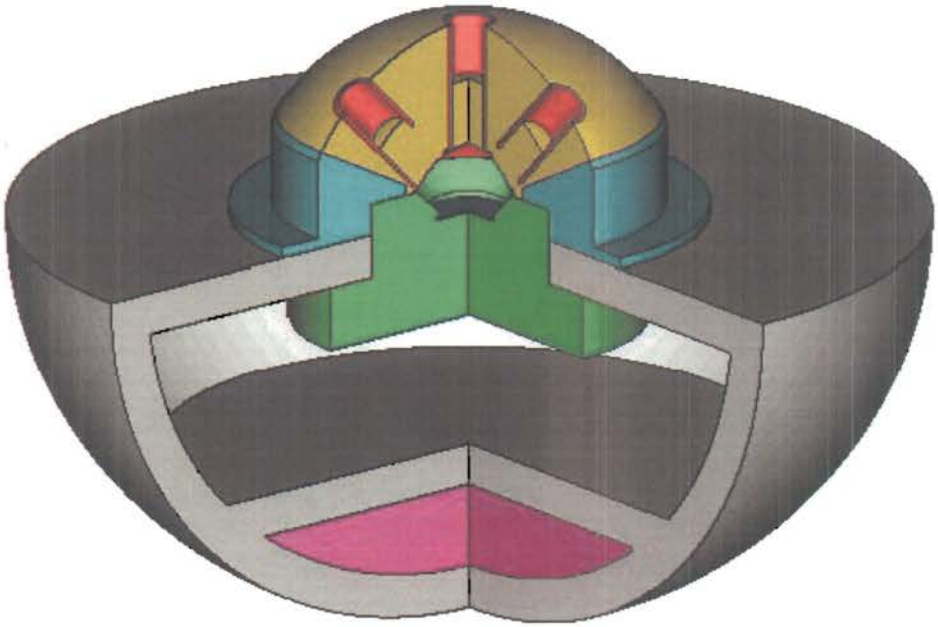

Figure 4. Saltshaker shield for channel 6 as flown on the BDD-IIR on NS41

Each of the dome or saltshaker shields is a thick, inhomogeneous filter consisting of a thick outer shell of beryllium and a thin inner shell of gold (replaced angles greater than 55° by a titanium support ring). All of the outer beryllium hemispherical shells have the same outer and inner radii, 2.3393 cm and 0.8585 cm, respectively. The inner radius of the gold shell is 0.8179 cm. (One of the two solid dome shields is identical to the beryllium and gold shields used for the four saltshakers except that it has no collimators; the second dome shield lacks the inner layer of gold.) Each saltshaker shield was made by drilling through the hemispherical shell with a set of five identical, radially-oriented holes that were fitted with 0.05-cm-thick cylindrical collimating tubes of gold. The diameter of the collimating apertures in each shield was scaled up with the threshold energy of that channel so that the expected counting rates in all channels would be comparable. Channels 3, 4, and 5 use reentrant collimating tubes of length 1.83 cm; channel 6 uses 1.52-cm-long collimating tubes. The hole diameter plus the channel's geometric gathering power, G, as determined by the collimators are listed in Table I.

Table I.

Physical Characteristics of the 8 BDD-IIR Channels

Channel Number	Filter Material	Filter Thickness (mm)	Number of Holes	Hole Diameter (mm)	Geometric Factor (cm^2 sr)
1	Mylar/Al	0.00152[a]	1[b]	0.305	6.21×10^{-4}
2	Be	0.254	1[b]	0.305	6.21×10^{-4}
3	Be	0.737	5	1.500	4.64×10^{-4}
4	Be	1.829	5	1.900	1.19×10^{-3}
5	Be	3.962	5	2.400	3.03×10^{-3}
6	Be	7.874	5	4.445	4.99×10^{-2}
7	Be	14.808[c]	0	--	1.34
8	Be +Au	14.808[c] +0.406[c]	0	--	1.34

[a] 1.52-μm Mylar with both sides aluminized to 1200 Angstroms.

[b] Conical collimator.

[c] Shield only, no holes and filters used.

Beryllium filters that are inserted and glued into the exit aperture of each collimator determine the incident-energy threshold of the channel for electrons and protons. The thicknesses of the filters are given in Table I. The energy characteristics of the eight BDD-IIR channels, listed in Table II, are derived from the mechanical characteristics (given in Table I) and the deposited-energy threshold of the silicon sensor elements. Because electrons scatter and straggle more while passing through matter than do protons, the range of energies over which penetration occurs is greater with incident electrons compared with incident protons. However, achieving and maintaining a light-tight interface between the gold collimator and the beryllium filter proved to be too much of a challenge for the simple glue-together construction method attempted with this design, especially where small-diameter holes and thin filters are involved

Table II.

BDD-IIR Penetration Energies (MeV)

Channel	Electrons[a]			Protons[b]		
	12%	50%	88%	12%	50%	88%
1	0.08	0.08	0.13	1.27	1.27	1.27
2	0.21	0.25	0.36	5.27	5.32	5.37
3	0.40	0.48	0.66	9.37	9.46	9.55
4	0.76	0.90	1.21	15.6	15.8	16.0
5	1.39	1.64	2.16	24.1	24.3	24.5
6	2.47	2.88	3.69	35.2	35.5	35.8
7	4.26	4.97	6.18	50.0	50.4	50.9
8	5.67	7.57	10.9	53.7	54.1	54.6

[a] Energy for which the given percentage of incident electrons emerge from the filter with >0.074 MeV.

[b] Energy for which the given percentage of incident protons emerge from the filter with >1.16 MeV.

One of the two conical collimators listed in Tables 1 and 2 (channel 2) is depicted in Fig. 5 using a slightly different color scheme than in Figs. 1 to 4. Here, the silicon sensor element is shown in purple; beryllium filter, yellow; **tantalum** aperture, **blue**; aluminum collimator body, instrument housings, and sensor deck, gray; plastic insulation, green; and lumped mass below the sensor deck; magenta. The basic design shown here was subsequently adapted to provide robust replacements for the four saltshaker shields on two modified instruments (these are described in Section 3 of this report).

The conical collimator features a precision aperture machined from 2-mm-thick tantalum within an aluminum body. Except for the different filters behind the exit aperture, channels 1 and 2 are mechanically identical. (The thickness of the filter determines the energy ranges covered by the channel.) These collimators feature a 110° field of view and a 0.0305-cm diameter tantalum aperture to reduce the very large flux of electrons >77 keV and >210 keV to an acceptable level. A light-tight window of aluminized Mylar (1200 Angstroms of aluminum deposited on each side of 1.52-μm-thick Mylar) covers

the entrance of the conical collimator and also serves as a dust cover for the conical hole. The filter for channel 1 consists of the same aluminized Mylar used for the light-tight windows; channel 2 uses 0.0254-cm-thick beryllium for a filter.

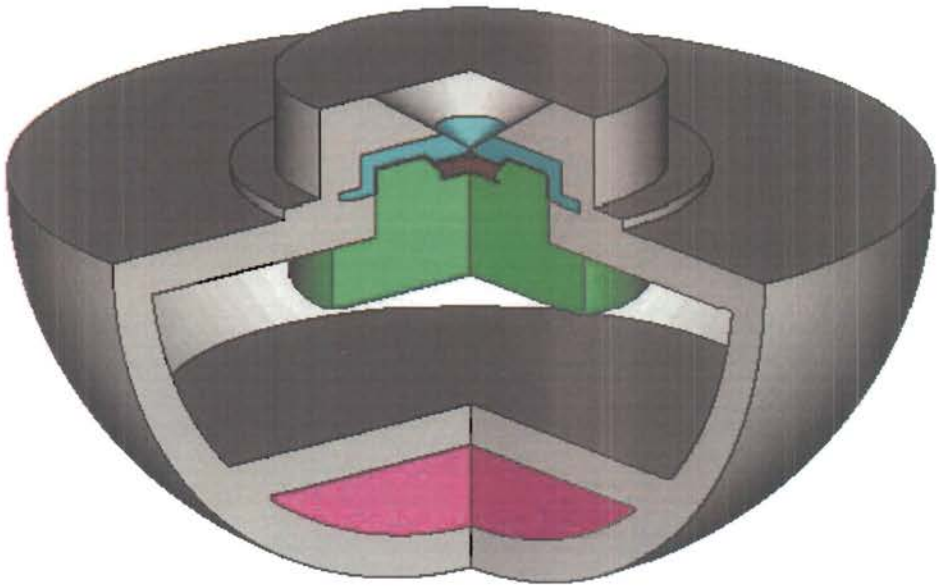

Figure 5. Conical collimator for channel 2 as flown on the BDD-IIR on NS41. Here the color blue denotes the material tantalum.

2. BDD-IIR Performance

As mentioned at the beginning of this report, the first BDD-IIR instrument that flew aboard GPS NS41 recorded data in channel 3 (both the electron and the proton data) that was heavily contamination by sun light. The interface between the gold collimating tube and the beryllium filter glued upon its exit aperture was identified definitively as the location of the light leak. Furthermore, the qualification test plan did not verify immunity to sun light (light tightness) following vibration and thermal cycling, but only after final assembly of the BDD-IIR unit. The underlying design of the saltshaker shields itself was deemed to be too simple to guarantee light-tight interfaces.

The on-orbit performance of the first BDD-IIR also verified the prediction (from Monte Carlo simulations) of a significant bremsstrahlung component to the channel response. The response of electron detectors of the "filter/sensor" type extend to energies lower than the filter penetration energy, e.g., Table I. Although incident electrons of energy less than the penetration energy may stop completely in the filter, a fraction of their incident energy is radiated as bremsstrahlung photons; once produced, a photon may interact and deposit energy in the sensor element itself; if the energy deposition exceeds the threshold for the channel a count will be scored. The energy spectrum of

bremsstrahlung photons forms a continuum extending from the energy of the incident electrons down to zero; both the magnitude and the hardness of the spectrum depend on the material in which the incident electrons interact. As an illustrative example, two components of the response function for a "filter/sensor" type are plotted in Fig. 6; these response functions correspond to BDD-IIR channel 6 (the geometry shown in Fig. 4); plotted with the blue line is the response resulting from electrons incident upon the just beryllium dome and the titanium ring; plotted with the red line is the response resulting from electrons incident upon the aluminum annulus and the hemispherical back; both components features a "bremsstrahlung nose" that extends below the penetration energy of the filter (~2.5 MeV) or the shielding (~6.5 MeV) down to the deposited-energy threshold for the active element. Above ~5.7 MeV, electrons incident on the beryllium and gold hemispherical shell penetrate the dome and produce the second step-like increase in the dome component of the response.

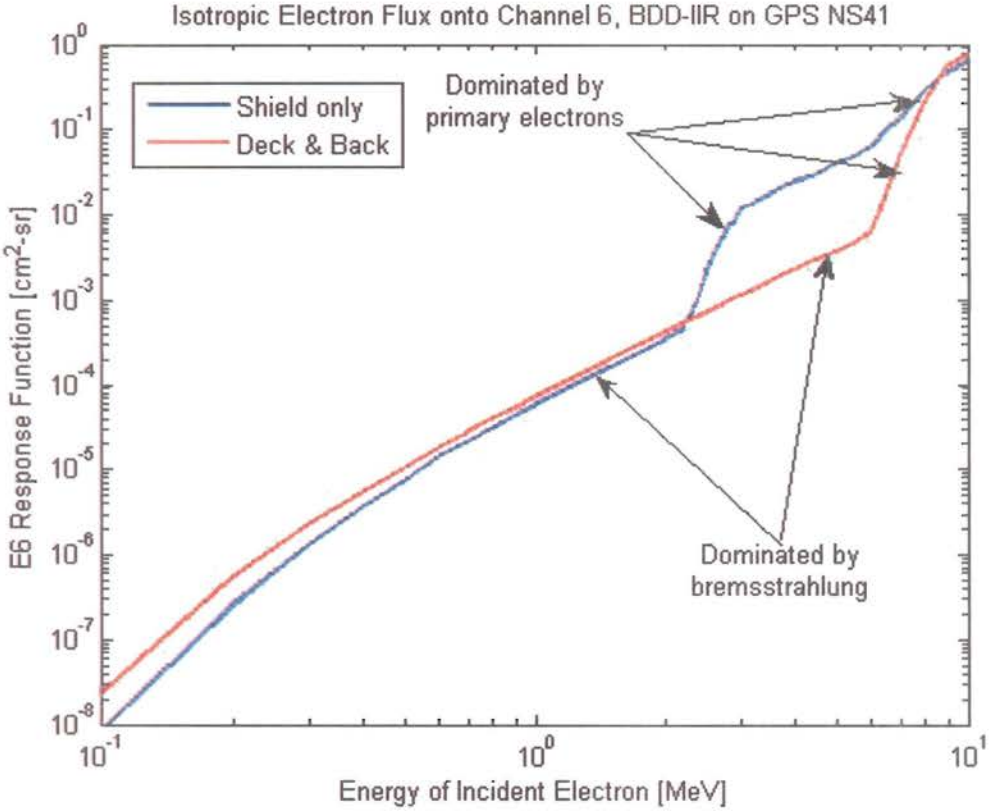

Figure 6. Computed responses of the BDD-IIR channel E6 (E_{dep} > 0.09373 MeV) to incident isotropic fluxes of monoenergetic electrons.

The contributions of the aluminum hemispherical back and annular deck were included in all the BDD-IIR responses after a detailed numerical study of the "bremsstrahlung nose" of the shield response revealed that **80%** of this signal originated from electrons incident on the **titanium** support ring (blue in Figs. 1 to 4), contrary to the expectation that the beryllium portion (yellow in Figs. 1 to 4) should dominate. This revelation that a significant contribution to the response originated from an unexpected place, prompted a more detailed evaluation of bremsstrahlung originating in the sensor housing, electronics box, and spacecraft (modeled here as a simple hemispherical shell and annular deck).

Finally, because of the proximity of the silicon detector elements to the gold collimators and the gold inner shields, all of the BDD-IIR lower-level discriminators were operated at 93 keV (level 2) rather than 74 keV (level 1) in order to avoid features associated with the K-edge of the nearby gold.

3. Modified Collimators

In response to the identified vulnerability to light leaks, the two remaining BDD-IIR instruments were modified by replacing all of the collimators of the saltshaker type by new ones of a more robust design, with identical masses and fabricated mostly from spare parts. In addition to eliminating light leaks, the new collimators are designed to improve the contrast between the direct electron component and the secondary bremsstrahlung component of the detector response. The new design modifies the conical collimator shown in Fig. 5 by accommodating thicker beryllium filters above the tantalum apertures. Light is excluded by both an O-ring seal between the aluminum housing and the tantalum aperture and a light-tight window/dust cover at the top of the conical hole. Again, aperture size is scaled up with filter thickness, and the geometrical gather power, G, is increased to increase the sensitivities to penetrating electrons compared with the bremsstrahlung contribution mainly from the deck and back. Mechanical details about the modified collimators are given in Table III; they are depicted in Figs. 7 to 10.

Table III.

Physical Characteristics of the 8 BDD-IIRM Channels

Channel Number	Filter Material	Filter Thickness (mm)	Number of Holes	Hole Diameter (mm)	Geometric Factor (cm^2 sr)
1	Mylar/Al	0.00152[a]	1[b]	0.305	6.21×10^{-4}
2	Be	0.254	1[b]	0.305	6.21×10^{-4}
3	Be	0.737	1[b]	0.305	6.21×10^{-4}
4	Be	1.829	1[b]	0.533	1.90×10^{-3}
5	Be	3.962	1[b]	0.864	4.99×10^{-3}
6	Be	7.874	1[b]	3.454	1.21×10^{-1}
7	Be	14.808[c]	0	--	1.34
8	Be +Au	14.808[c] +0.406[c]	0	--	1.34

[a] 1.52-μm Mylar with both sides aluminized to 1200 Angstroms.

[b] Conical collimator.

[c] Shield only, no holes and filters used.

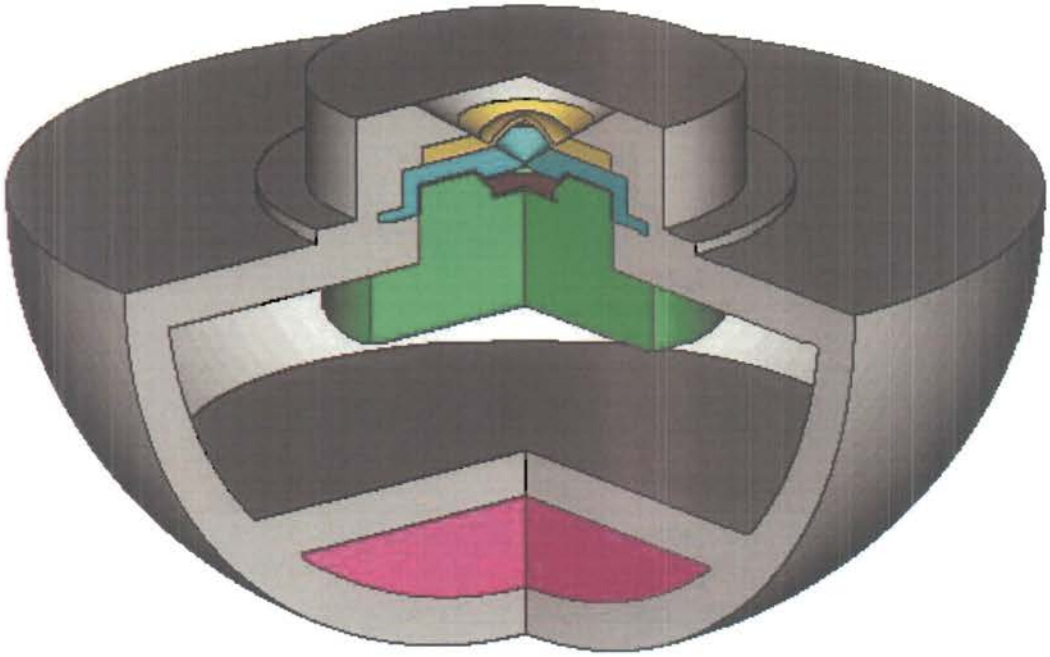

Figure 7. Conical collimator for channel 3 on the BDD-IIRM (SV08 and spare).

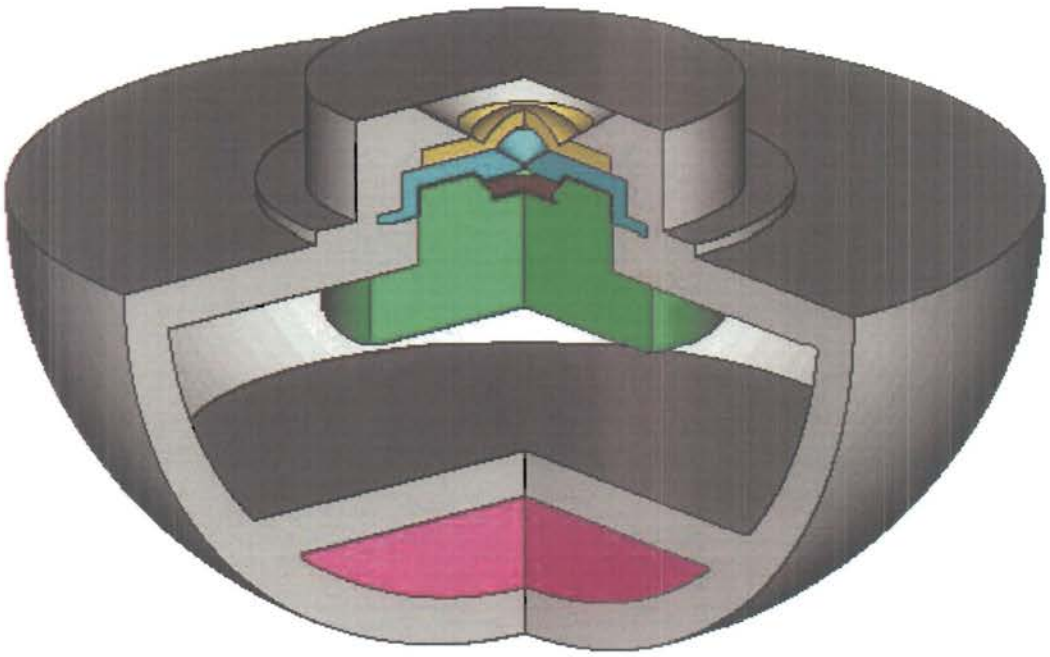

Figure 8. Conical collimator for channel 4 on the BDD-IIRM (SV08 and spare).

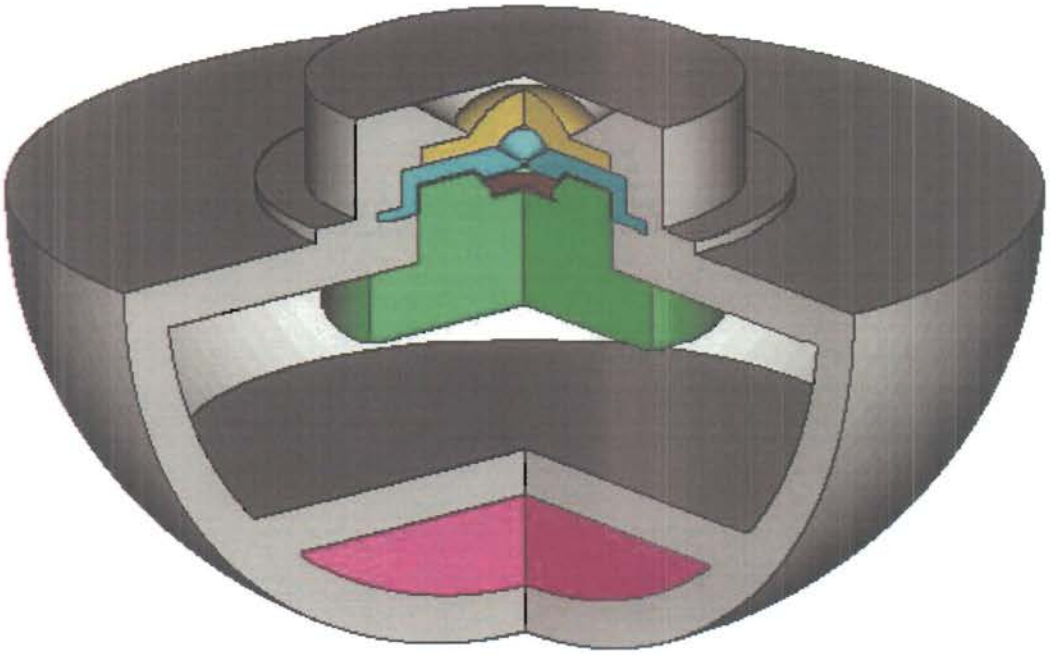

Figure 9. Conical collimator for channel 5 on the BDD-IIRM (SV08 and spare).

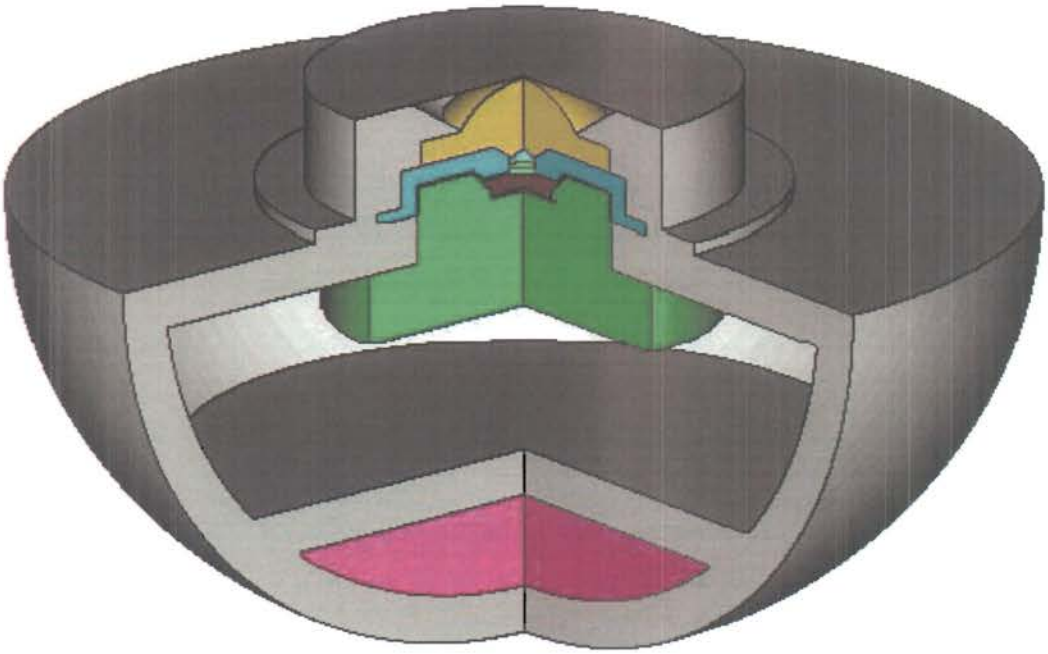

Figure 10. Conical collimator for channel 6 on the BDD-IIRM (SV08 and spare).

4. Numerical Modeling of Electron Responses

Flux response functions, in units of cm^2-sr, were calculated for each BDD-IIR channel using MCNP (Los Alamos Monte Carlo N Particle code)[3] to transport electrons and secondary photons through the simulation geometry. This state-of-the-art code handles complex three-dimensional geometries filled with multiple materials. MCNP is part of the Los Alamos Radiation Transport Code System and is maintained by the Diagnostics and Applications Group, X-5, at Los Alamos National Laboratory. The code compiles single-parameter pulse-height distributions of the energy deposited by all primary and secondary electrons and photons in the active volume of the silicon detector. Electron response functions were then evaluated from these pulse-height tallies; two examples are plotted in Fig. 6. Integration of the response functions with appropriate incident electron spectra yields the channel counting rates that may be compared directly with the measured data.

A. Source used to compute response functions: The source used to compute detector responses was an isotropic flux (realized by emitting a "cosine-current" from each element of source surface area) of monoenergetic electrons incident upon the simulation geometry. To realize isotropic fluxes electrons were emitted from a spherical surface concentric with, but larger than, the simulation volume. The emission was uniform from each element of surface area and, with respect to the unit normal of each area element (i.e., the inward pointing radius vector), the integral probability of emission was directly proportional to the polar angle's sine squared such that the "phase-space" associated with the incident electrons is $A_s \times \pi$ [cm^2-sr], where A_s is the source area. (Each area element emits electrons non-uniformly into an average of π ster-radians.)

B. Geometry: Schematic drawings of the first flight BDD-IIR are shown in Figs. 1 to 4. The various colors indicate the materials of which the BDD-IIR instrument is constructed, as follows. The silicon sensor element is shown in purple; beryllium shield and filters, yellow; gold shield and collimators, red; titanium support ring, blue; plastic insulation, green; and lumped mass below the sensor deck; magenta. The aluminum instrument housing and sensor deck (approximated here as a simple hemispherical shell and annulus) are shown in gray. Likewise, schematic drawings of the modified BDD-IIRM instruments are shown in Figs. 7 to 10, using a somewhat different color scheme. The silicon sensor element is shown in purple; beryllium shield and filters, yellow; tantalum aperture, blue; plastic insulation, green; and lumped mass below the sensor deck; magenta. The aluminum aperture housing is shown in gray, as are instrument housing and the sensor deck.

C. Response functions: Deposited-energy spectra were compiled for incident electrons in the energy range 0.1 to 10 MeV. This was accomplished by the pulse-height tally mentioned above which yields the fractions of the average incident electron that score in the specified deposited-energy bins. Pulse-height spectra were recorded at 5-keV resolution for post-processing; a deposited-energy spectrum that included contributions from the entire cascades generated by individual source electrons was recorded for each incident electron energy. Multiplication of these fractions by the "phase-space" of the

incident distribution of electrons, πA_s, gives the absolute channel responses in the units of cm^2-sr.

The analog and digital electronics of the BDD-IIR classifies and scores counts according two threshold levels, a lower-level discriminator (LLD) threshold and an upper-level discriminator (ULD) threshold. Any deposition greater than or equal to the LLD threshold and less than the ULD threshold contributes to the "electron" response; depositions greater than or equal to the ULD threshold score in the "proton" channel.

Absolute calibration of the deposited-energy thresholds was accomplished through use of radioactive sources and a precision pulser as follows. First, with the shields removed and a radioactive source placed directly over one of BDD-IIR's sensors, the positions of the 59.5-keV americium-241 gamma ray and the 481-, 561-, 975-, and 1047-keV bismuth-207 electron lines were recorded in a multichannel analyzer (MCA) attached to the output of BDD-IIR's first amplifier stage. The radioactive source was then removed. Next, the combination of the precision pulser and the injection capacitor for the channel was calibrated by matching each source feature recorded by the MCA. The MCA was then removed, and the thresholds associated with the channel were carefully mapped with the calibrated pulser. The threshold maps were least-squares fitted to determine a central energy and an equivalent full-width-at-half-maximum (FWHM) parameter for each threshold. (For an error-function-like transition, these parameters are defined in terms of the 50% point and the distance between the 12% and 88% points, respectively.)

Tables IV summarizes the measured thresholds for channels 3 to 6 for the first BDD-IIR flight unit.

Table IV.
Discriminators Thresholds for BDD-IIR on NS41

Channel	LLD Deposited Energy (keV)	LLD FWHM (keV)	ULD Deposited Energy (keV)	ULD FWHM (keV)
3	89.9	17.2	1134	17.2
4	94.3	19.4	1163	19.2
5	93.4	27.3	1149	25.8
6	93.7	15.9	1180	14.5

Tables V summarizes the measured thresholds for channels 3 to 6 for the modified BDD-IIR that is slated to fly on GPS SV08.

Table V.
Discriminator Thresholds for BDD-IIRM on SV08

Channel	LLD Deposited Energy (keV)	LLD FWHM (keV)	ULD Deposited Energy (keV)	ULD FWHM (keV)
3	88.9	18.2	1117	17.4
4	94.0	18.8	1176	19.8
5	94.9	21.3	1182	19.3
6	95.6	18.3	1201	17.4

The response functions for the two versions of channel 3 are compared in Fig. 11. The blue curve was evaluated using the geometry shown in Fig.1 and the threshold parameters of Table IV; the green curve, the geometry shown in Fig. 7 and the threshold parameters of Table V. The high-Z material used in the new design suppresses both the low-energy bremsstrahlung "nose" and the contribution of penetrating primary electrons at high energy; as expected, the larger aperture of the new design increases the response to in-the-aperture electrons.

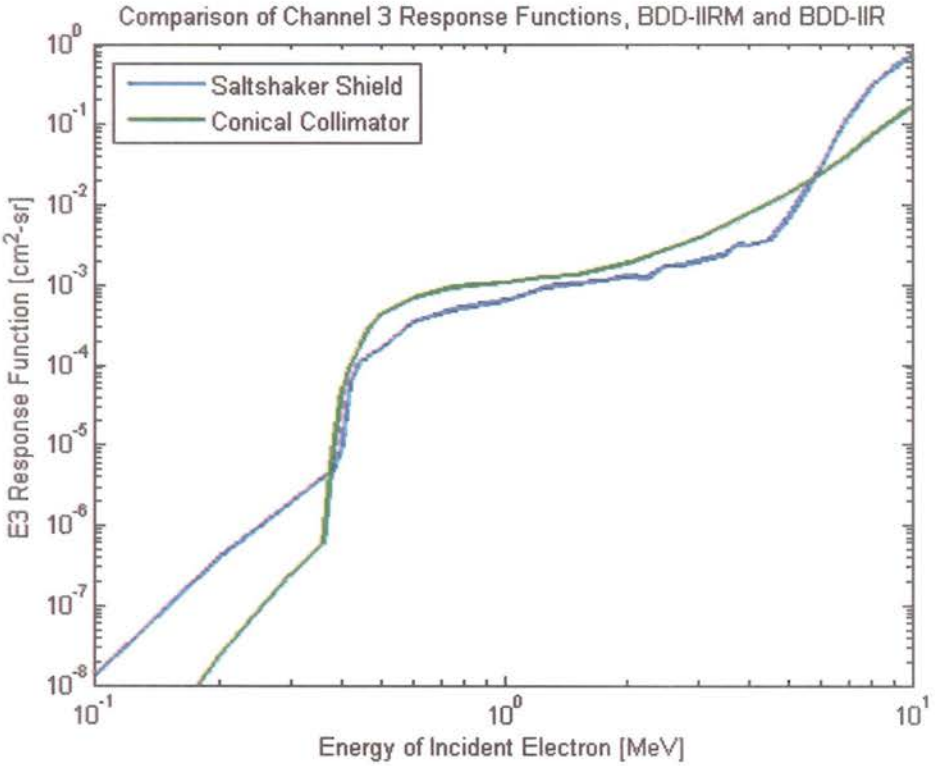

Figure 11. Computed responses of conical collimator and saltshaker shield version of channel E3 to incident isotropic fluxes of monoenergetic electrons.

The response functions for the two versions of channel 4 are compared in Fig. 12. The blue curve was evaluated using the geometry shown in Fig.2 and the threshold parameters of Table IV; the green curve, the geometry shown in Fig. 8 and the threshold parameters of Table V. The high-Z material used in the new design suppresses both the low-energy bremsstrahlung "nose" and the contribution of penetrating primary electrons at high energy; as expected, the larger aperture of the new design increases the response to in-the-aperture electrons.

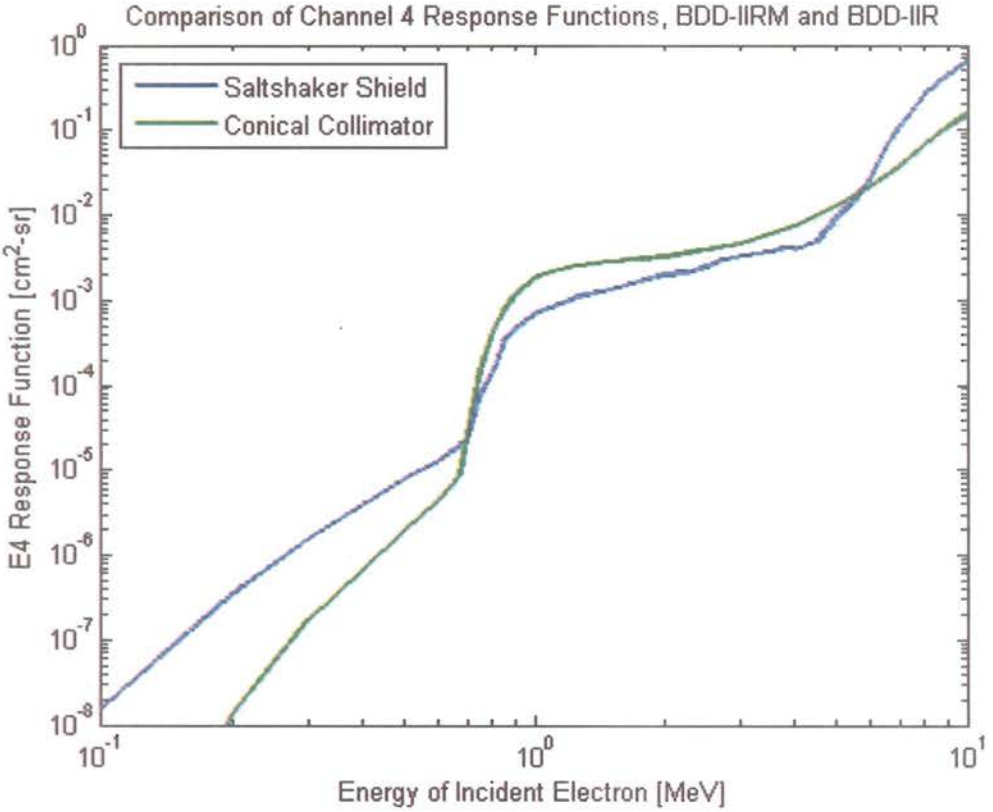

Figure 12. Computed responses of conical collimator and saltshaker shield version of channel E4 to incident isotropic fluxes of monoenergetic electrons.

The response functions for the two versions of channel 5 are compared in Fig. 13. The blue curve was evaluated using the geometry shown in Fig.3 and the threshold parameters of Table IV; the green curve, the geometry shown in Fig. 9 and the threshold parameters of Table V. The high-Z material used in the new design suppresses both the low-energy bremsstrahlung "nose" and the contribution of penetrating primary electrons at high energy; as expected, the larger aperture of the new design increases the response to in-the-aperture electrons.

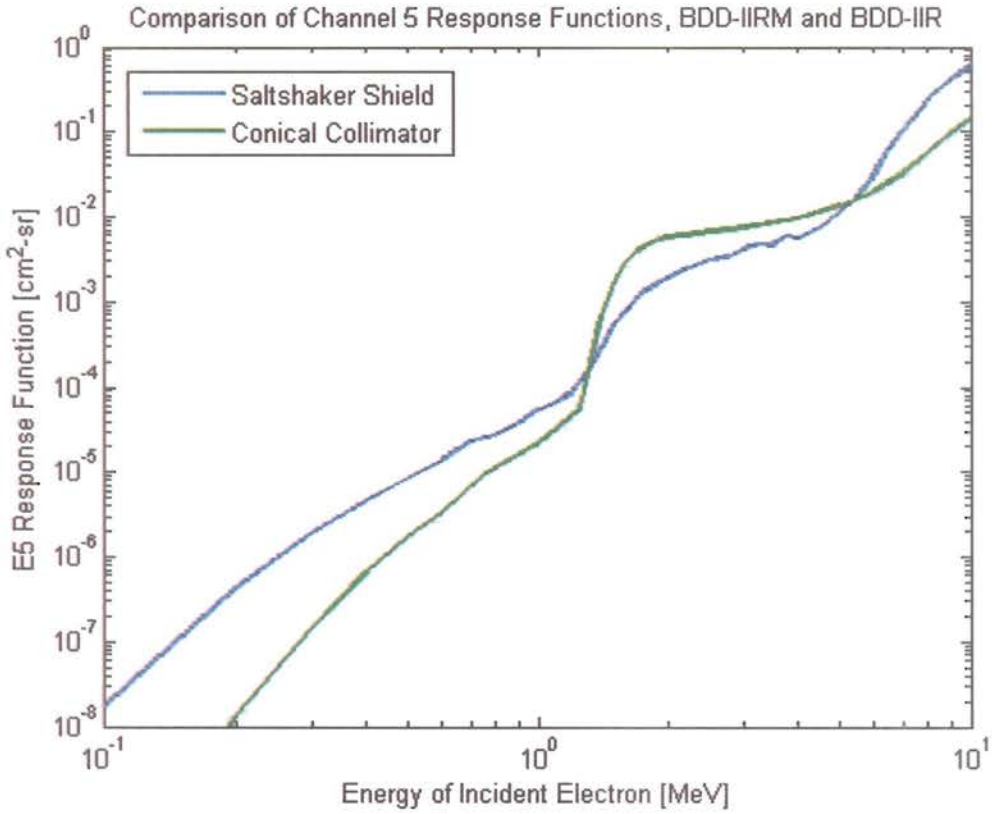

Figure 13. Computed responses of conical collimator and saltshaker shield version of channel E5 to incident isotropic fluxes of monoenergetic electrons.

The response functions for the two versions of channel 6 are compared in Fig. 14. The green curve was evaluated using the geometry shown in Fig.4 and the threshold parameters of Table IV; the blue curve, the geometry shown in Fig. 10 and the threshold parameters of Table V. The high-Z material used in the new design suppresses both the low-energy bremsstrahlung "nose" and the contribution of penetrating primary electrons at high energy; as expected, the larger aperture of the new design increases the response to in-the-aperture electrons.

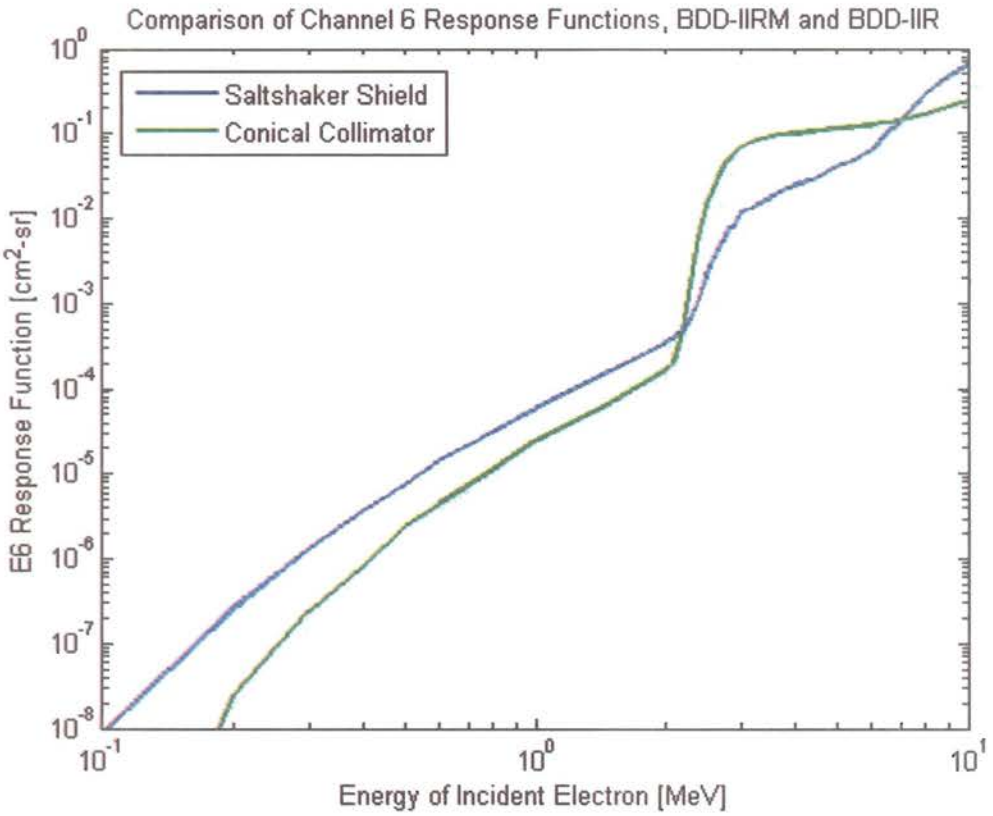

Figure 14. Computed responses of conical collimator and saltshaker shield version of channel E6 to incident isotropic fluxes of monoenergetic electrons.

The high-Z material used in the new design also affects the sensor responses to electrons incident upon the aluminum back and deck. The geometry of the plane surface of the tantalum in close proximity to the sensor elements is more favorable to both tertiary electron production by secondary photons in the tantalum itself, and reflection of teritiary electrons produced elsewhere that impinge upon the tantalum from below. No high-Z material shields the sensors from the bremsstrahlung photons produced below the sensor deck. The bremsstrahlung "nose" is not suppressed, but is actually enhanced somewhat in the few 100s keV energy range, because of enhanced photocathode emission and electron reflection at the sensor facing surface of the tantalum collimator.

Figures 15 to 18 show the two separate contributions, collimator (blue lines), and deck and back (red lines), to the total responses of the modified BDD-IIRM channels 3 to 6.

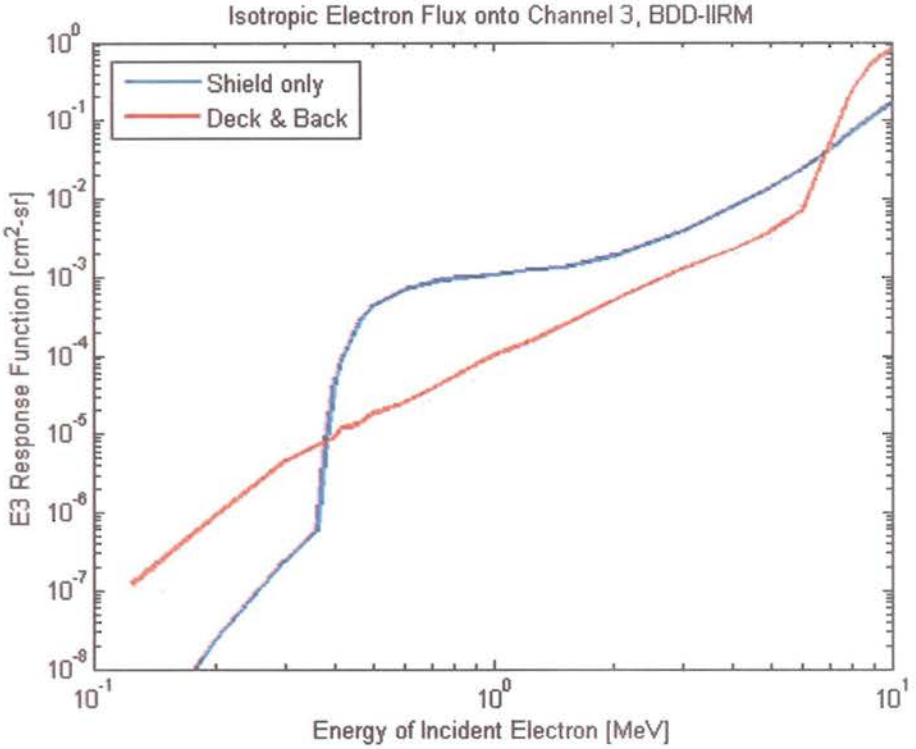

Figure 15. Computed responses of the BDD-IIRM channel E3 ($E_{dep} > 0.0889$ MeV) to incident isotropic fluxes of monoenergetic electrons.

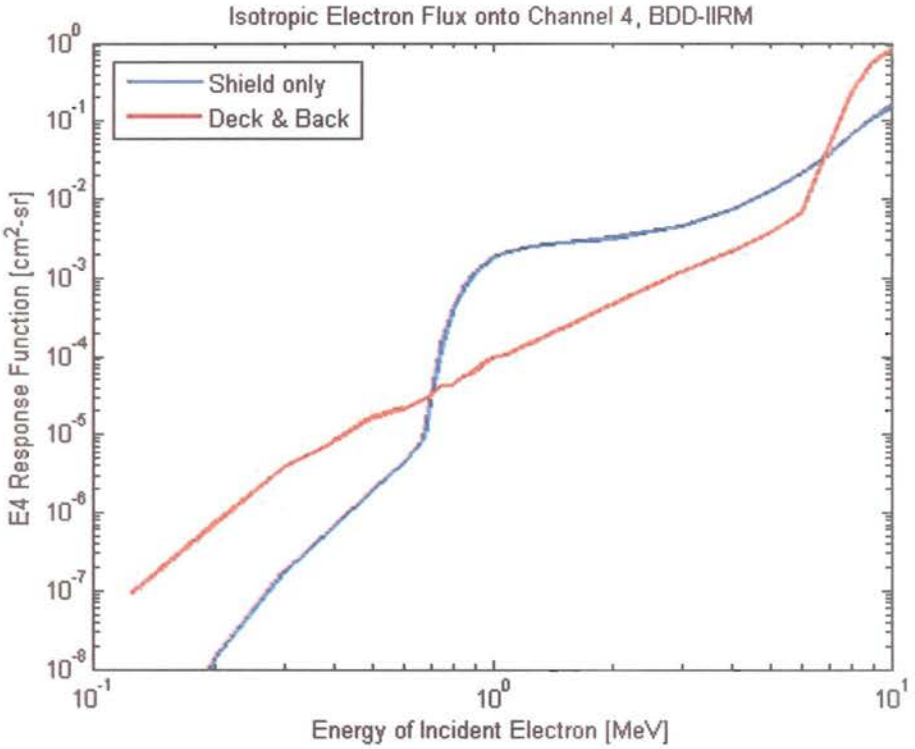

Figure 16. Computed responses of the BDD-IIRM channel E4 ($E_{dep} > 0.0940$ MeV) to incident isotropic fluxes of monoenergetic electrons.

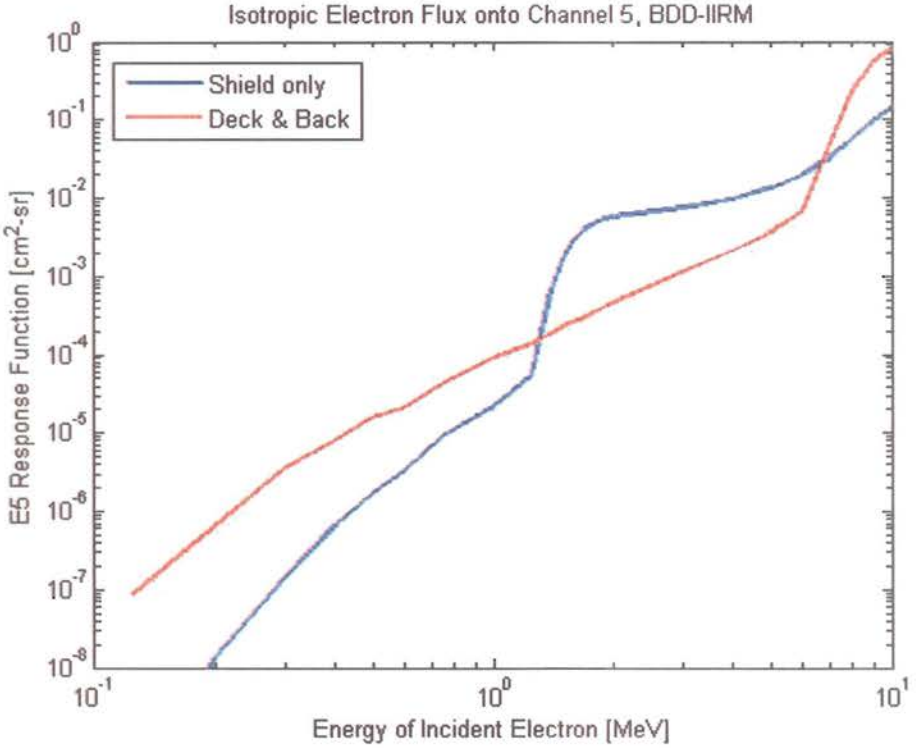

Figure 17. Computed responses of the BDD-IIRM channel E5 ($E_{dep} > 0.0949$ MeV) to incident isotropic fluxes of monoenergetic electrons.

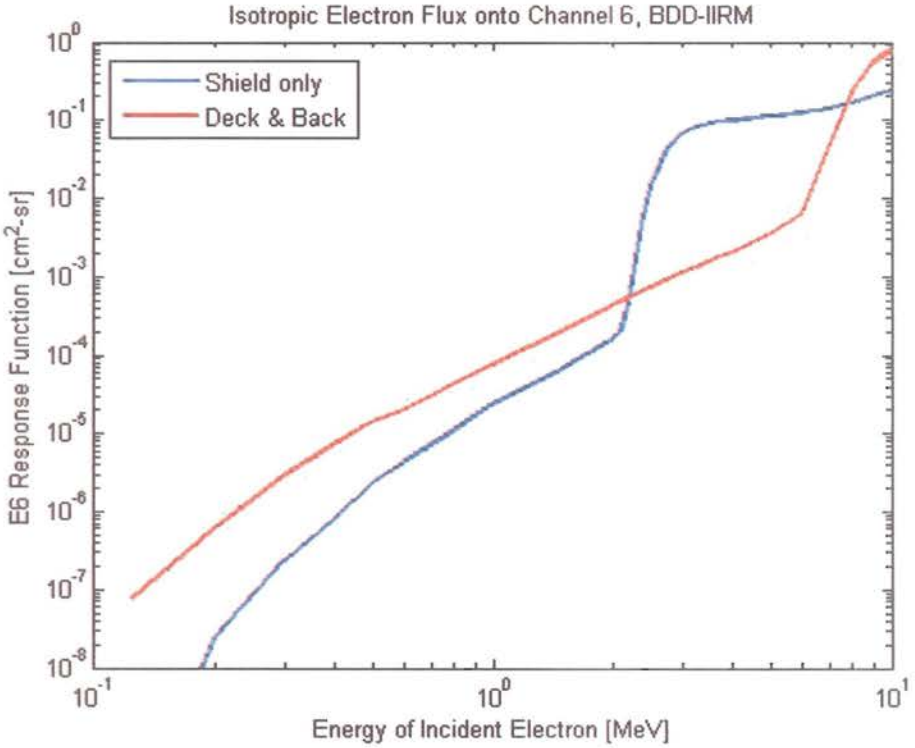

Figure 18. Computed responses of the BDD-IIRM channel E6 ($E_{dep} > 0.0956$ MeV) to incident isotropic fluxes of monoenergetic electrons.

Figures 19 to 22 compare the total responses, shield plus deck and back, for the original and the modified designs. Because the backs of the sensors are not shielded by high-Z material, the full spectrum of bremsstrahlung photons produced in aluminum impinges from below on both the silicon itself and the nearby material in front. The new configuration actually enhances the response from electrons incident on the deck and back, offsetting somewhat the benefit of the suppressed response from electrons incident on the shields themselves. Enclosing the backs of the sensors in 2mm-thick tantalum cans would have much more effectively suppressed the low-energy bremsstrahlung noses. The authors recommend that in future designs as much or more attention be paid to sensor backsides as to the collimators in front.

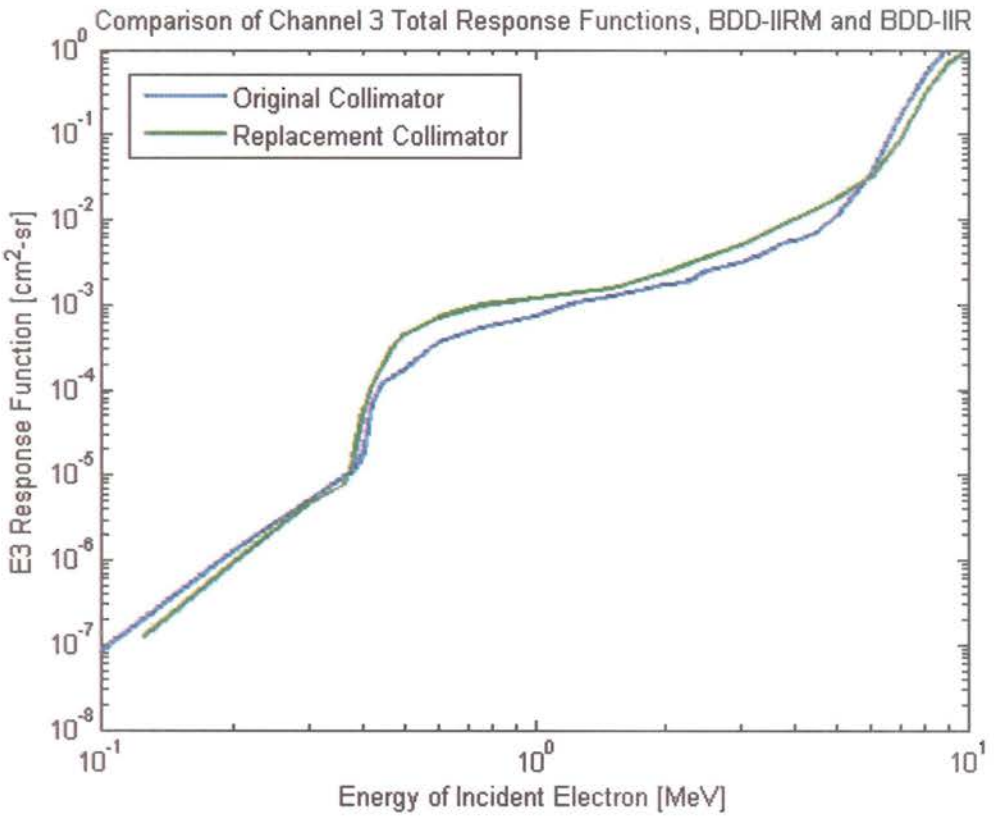

Figure 19. Computed total responses of conical collimator and saltshaker shield versions of channel E3 to incident isotropic fluxes of monoenergetic electrons.

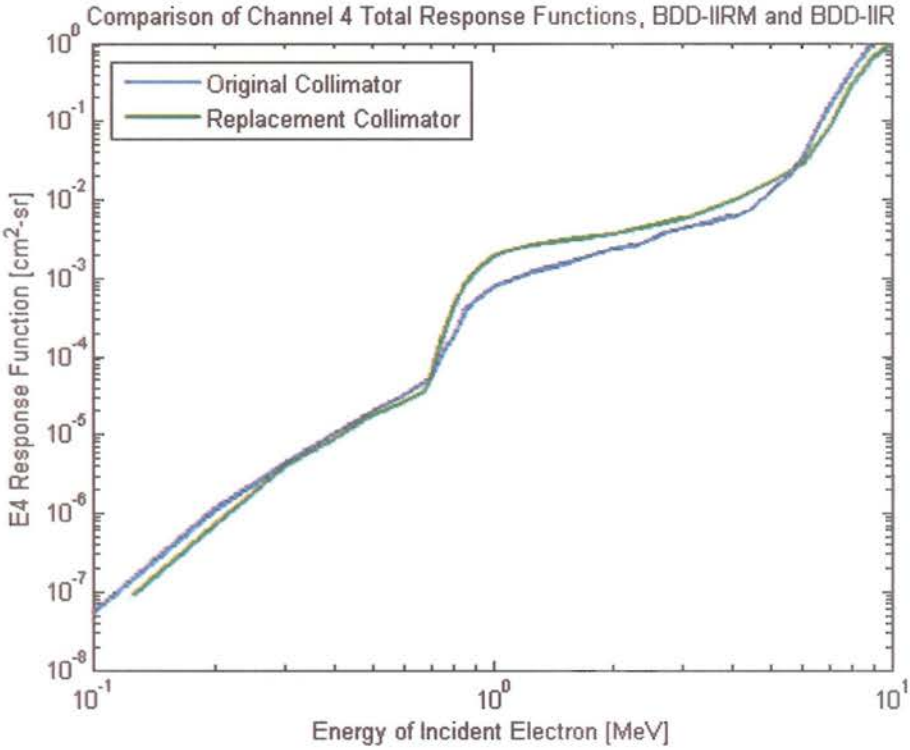

Figure 20. Computed total responses of conical collimator and saltshaker shield versions of channel E4 to incident isotropic fluxes of monoenergetic electrons.

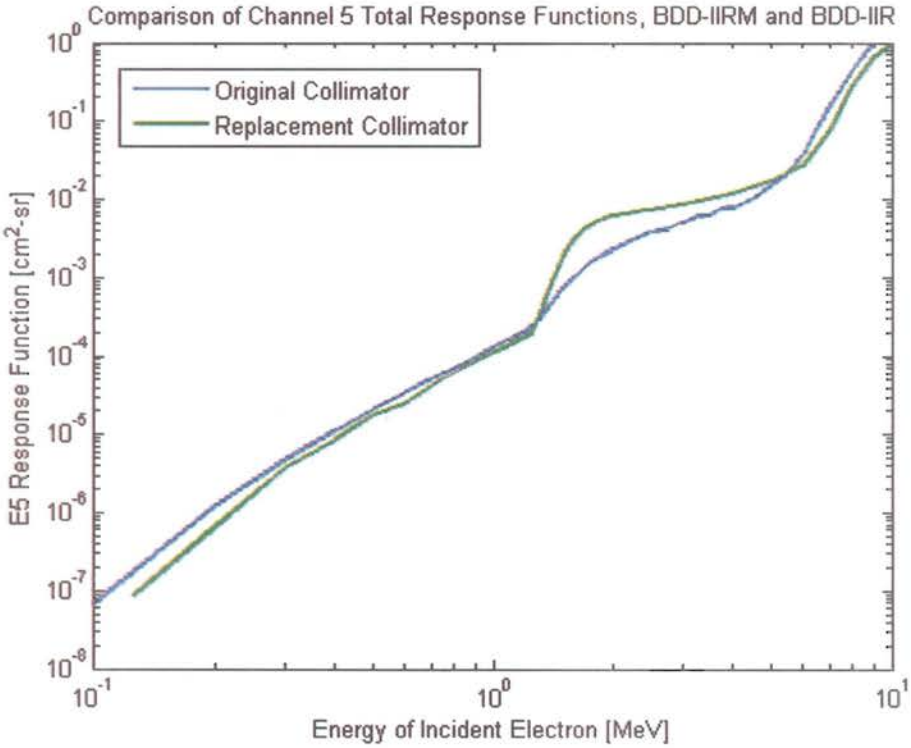

Figure 21. Computed total responses of conical collimator and saltshaker shield versions of channel E5 to incident isotropic fluxes of monoenergetic electrons.

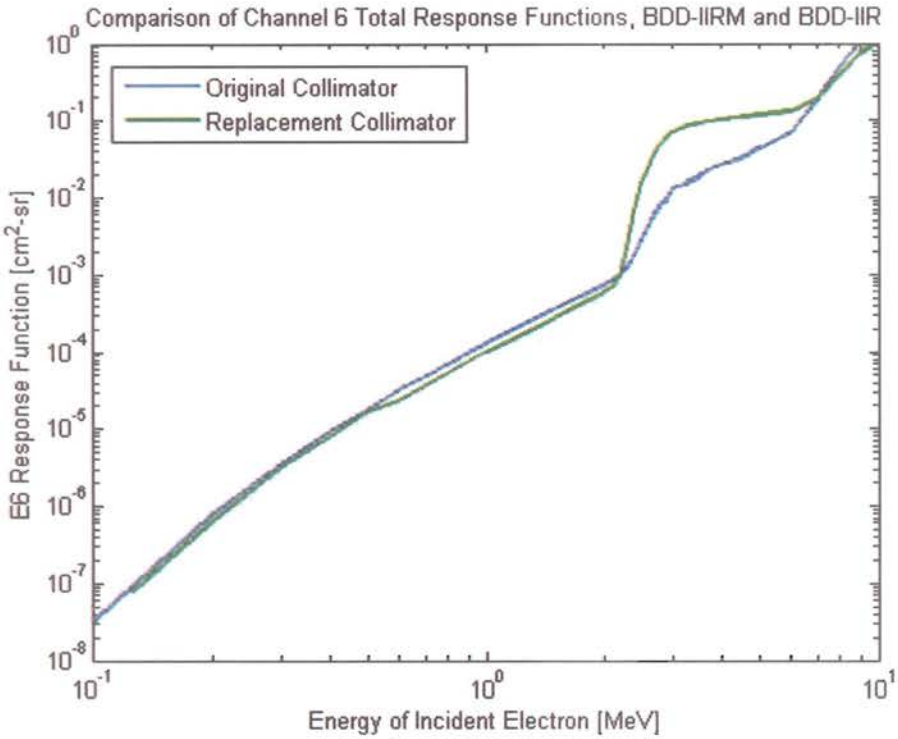

Figure 22. Computed total responses of conical collimator and saltshaker shield versions of channel E6 to incident isotropic fluxes of monoenergetic electrons.

5. Conclusion

The on-orbit performance of the first BDD-IIR (Burst Detection Dosimeter, Block IIR) instrument that flew aboard GPS NS41 (Global Positioning System satellite Navstar 41), demonstrated a design flaw in the "saltshaker" shields employed in four of the instrument's eight channels: sun light heavily contaminated the data reported by one of these channels. In response to the identified vulnerability to light leaks, the two remaining BDD-IIR instruments were modified by replacing all of the collimators of the saltshaker type by new ones of a more robust design, with identical masses and fabricated mostly from spare parts. In addition to eliminating light leaks, the new collimators were designed to improve the contrast between the direct-electron component and the secondary-bremsstrahlung component of the detector response. The original saltshaker shields of the BDD-IIR on NS41 were compared and contrasted with the replacement collimators deployed in the BDD-IIRM for the second flight unit and the flight spare. Because the backs of the sensors were not shielded by high-Z material, the full spectrum of bremsstrahlung photons produced in aluminum impinges from below on both the silicon itself and the nearby material in front. The new configuration actually enhances the response from electrons incident on the deck and back, offsetting somewhat the benefit of the suppressed response from electrons incident on the shields themselves. Enclosing the backs of the sensors in 2mm-thick tantalum cans would have much more effectively suppressed the low-energy bremsstrahlung noses. The authors recommend that as much or more attention be paid to sensor backsides as to the collimators in front.

References

1. T.E. Cayton, D.M. Drake, K.M. Spencer, M. Herrin, T.J. Wehenr, and R.C. Reedy, "Description of the BDD-IIR: Electron and Proton Sensors on the GPS", Los Alamos National Laboratory Report LA-UR-98-1162 (1998).

2. M.G. Tuszewski, T.E. Cayton, and J. C. Ingraham, "A New Numerical Technique to Design Satellite Energetic Electron Detectors", *Nuclear Instruments and Methods* **A482**, 653, 2002.